Software for adaptable eccentric analysis of confined concrete circular columns

Hayder A. Rasheed*[1], Ahmed M. Abd El-Fattah[2], Asad Esmaeily[1],
John P. Jones[3] and Kenneth F. Hurst[3]

[1]*Structural Engineering, Analysis and Mechanics Lab., Kansas State University, USA*
[2]*Dept. of Architecture, King Fahd University of Petroleum and Minerals, Dhahran, Saudi Arabia*
[3]*Bridge Design Office, Bureau of Design, Kansas Department of Transportation, USA*

Abstract. This paper describes the varying material model, the analysis method and the software development for reinforced concrete circular columns confined by spiral or hoop transverse steel reinforcement and subjected to eccentric loading. The widely used Mander model of concentric loading is adapted here to eccentric loading by developing an auto-adjustable stress-strain curve based on the eccentricity of the axial load or the size of the compression zone to generate more accurate interaction diagrams. The prediction of the ultimate unconfined capacity is straight forward. On the other hand, the prediction of the actual ultimate capacity of confined concrete columns requires specialized nonlinear analysis. This nonlinear procedure is programmed using C-Sharp to build efficient software that can be used for design, analysis, extreme event evaluation and forensic engineering. The software is equipped with an elegant graphics interface that assimilates input data, detail drawings, capacity diagrams and demand point mapping in a single sheet. Options for preliminary design, section and reinforcement selection are seamlessly integrated as well. Improvements to KDOT Bridge Design Manual using this software with reference to AASHTO LRFD are made.

Keywords: confined analysis; circular columns; eccentric loading; adjustable constitutive model; extreme events.

1. Introduction

The problems of truck overloads and truck impacts to reinforced concrete bridge piers are very common to State Departments of Transportation in the US and the world. In specific cases of pier impact with or without apparent damage, it is desirable to have a reliable analysis tool that can be used to assess the actual ultimate capacity of the pier prior to developing a course of action. It is widely known that AASHTO LRFD dictates the requirement of ignoring the contribution of confinement to the ultimate capacity of concrete columns. This contribution could be quite significant especially for columns dominated by axial behavior. Prediction of the actual ultimate capacity of confined concrete columns requires specialized nonlinear analysis.

It is widely known that AASHTO LRFD Specifications involve very detailed design procedures that need to be checked for varying number of limit states making the task of the designer very tedious. Accordingly, it is important to develop software that guide the bridge designer through the LRFD design process and facilitate the preparation of reliable analysis/design documents.

---

* Corresponding author, Associate Professor, E-mail: hayder@ksu.edu

The software that is commercially available for column analysis and design is typically restricted to unconfined analysis. PCA or SP Column version 4.10 of Structure Point or Portland Cement Association (Structure Point LLC 2002-2011) is widely used for design of bridge piers, shear walls or typical frame elements. The results are presented in terms of P-M interaction diagrams. The latest version of the software supports ACI 318-05 and CSA A23.3-04. CSiCOL of Computers and Structures, Inc (Computers and Structures 2011) have similar capabilities of SP Column with unlimited number of load combinations. The software supports ACI 318-02, BS8110 and CSA A-23.3-94 codes. Section Builder version 8.1.5 of Computers and Structures, Inc (Computers and Structures 2006) has the capability of introducing a user defined stress-strain model. However, all the confined concrete models available in literature cannot adjust the confined strength or ultimate strain based on the compression zone size or the eccentricity, which makes their predictions on the un-conservative side.

Software development of advanced phenomena in concrete members and structures could be recently found in several applications. This includes the deflection of shear walls (Kara and Dundar 2009a), of beams (Kara and Dundar 2009b), bond strength (Tanyildizi 2009) and crack determination (Kim *et al.* 2009). However, the applications, related to concrete column analysis and design, are limited. Tayem and Najmi (1996) inaccurately utilized Whitney stress block in circular cross section analysis since it was originally developed for rectangular cross sections. Samra *et al.* (1997) accounted for eccentric loading by varying the ultimate strain seen by extreme fibers, such that the internal moment balanced the applied one. However no evidence that the ultimate strain calculated based on Mander's ultimate strain can be reached before concrete crushing. Milton de Araújo (2001) used the probabilistic finite element analysis of reinforced concrete columns considering the Gaussian random variations in concrete and steel parameters as well as dimensions and axial loads. Monte Carlo simulations and partial safety factors were used to evaluate safety by means of the reliability index. It was shown that the variability of parameters has a significant effect on reliability. Kwon and Spacone (2002) modified Balan *et al.* (2001) hypoplastic-based concrete model utilizing the equivalent uniaxial strains proposed by Darwin and Pecknold (1977). The model developed was incorporated in FE software and showed good agreement with experimental results. Braga *et al.* (2006) developed analytical model based on the elasticity theory to predict the confining pressure in stirrups and internal lateral ties for square and circular cross section columns. This model was extended to be applied to circular cross section columns confined with FRP. Yeh and Chang (2007) developed a finite element procedure to predict the compressive strength and ultimate axial strain of CFRP confined circular concrete columns and to study the confinement efficiency in facilitating the design of CFRP retrofit. Anwar and Qaasim (2009) have conducted a parametric study to identify the optimum reinforced concrete column cross section for strength and ductility. They used Section Builder software with the user-defined stress strain feature which is applicable only to concentric loading while it is un-conservative for eccentric loading. More recently, Aschheim *et al.* (2010) developed a simple design procedure for determining the cross section dimensions for a given load combination acting on principal axes. Carpinteri *et al.* (2011) developed a numerical procedure for generating interaction diagrams based on the integrated cohesive/overlapping crack model in order to account for size effect. Song and Lu (2011) presented a study on the use of high fidelity finite element models for the investigation of the behavior of concrete confined by stirrups, as well as the interpretation of the numerical results. Oreta and Ongpeng (2011) presented a study using artificial neural networks to predict the compressive strength of circular reinforced concrete columns confined with both transverse steel and CFRP wrapping.

This study is intended to develop a detailed design and analysis procedure and user-friendly software based on AASHTO LRFD considering an auto-adjustable stress-strain curve based on the eccentricity of the axial load or the size of the compression zone. The developed and benchmarked software will also be used to assess the actual ultimate capacity of bridge piers requiring evaluation or capacity upgrade due to corrosion, overloads or truck impacts.

2. Materials and methods

2.1 Confined material model for eccentric loading

It has been recently recognized that the effective ultimate strength and strain of confined concrete subjected to eccentric load must vary with eccentricity (Esmaeily and Lucio 2002, Fam *et al.* 2003). This is caused by the reduction in those two values under higher eccentricity due to the reduction in the effective size of compression zone. Accordingly, an eccentricity model is proposed herein to account for this variation between the fully confined section case (f'_{cc}, ε_{cu}) at pure axial force and the fully unconfined section case (f'_c, 0.003). In order to map the variation between those two extreme cases to generate a certain stress-strain curve for a certain eccentricity, the widely known Mander model is used (Mander *et al.* 1988). This model yields the two extreme cases but nothing in between. The proposed stress-strain curve based on the Mander framework is expressed as, Fig. 1

$$f_c = \frac{\bar{f}_{cc}\bar{x}\bar{r}}{\bar{r}-1+\bar{x}^{\bar{r}}}$$ (1)

where $\bar{r} = \dfrac{E_c}{E_c-\bar{E}_{sec}}$, $\bar{E}_{sec} = \dfrac{\bar{f}_{cc}}{\bar{\varepsilon}_{cc}}$, $\bar{x} = \dfrac{\varepsilon_c}{\bar{\varepsilon}_{cc}}$, $E_c = 57000\sqrt{f'_c}$ in psi., $\bar{f}_{cc}$ is the strength of the partially confined eccentrically loaded concrete and $\bar{\varepsilon}_{cc}$ is the strain corresponding to $\bar{f}_{cc}$

$$\bar{f}_{cc} = \frac{1}{1+\dfrac{e}{D}}f'_{cc} + \frac{1}{1+\dfrac{D}{e}}f'_c$$ (2)

$$\bar{\varepsilon}_{cc} = \varepsilon'_c\left(1+5\left(\frac{\bar{f}_{cc}}{f'_c}-1\right)\right)$$ (3)
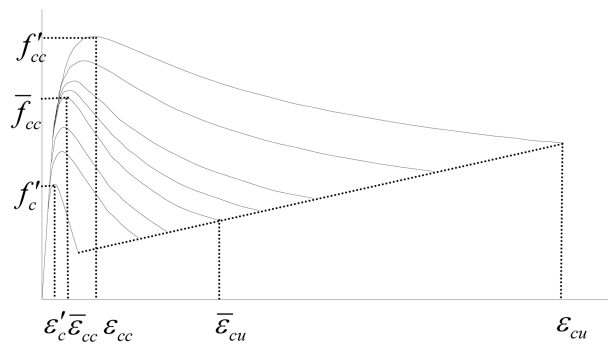

Fig. 1 Eccentricity model for stress-strain curves

where e is the radial eccentricity of the axial force, D is the column diameter, f_{cc}' is the strength of the fully confined concentrically loaded concrete determined based on the equations of Mander *et al.* (1988), f_c' is the strength of uniaxial unconfined compression and ε_c' is the strain corresponding to f_c'. Note that this material model is robust in the sense that $\overline{f_{cc}}$ and $\overline{\varepsilon_{cc}}$ converge to f_{cc}' and ε_{cc} in the upper extreme. They also converge to f_c' and ε_c' in the lower extreme.

The ultimate strain of the eccentric stress-strain curve is assumed to be the point of intersection of that curve with a straight line connecting the ultimate strain of the fully confined and unconfined compression, Fig. 1. This will gradually decrease the ductility from the fully confined case of axial compression to the unconfined case of pure bending. This will also lead to a robust transition between the two extremes. By equating the locus of the point of intersection between the straight line and the curve, a nonlinear equation in ultimate strain $\overline{\varepsilon}_{cu}$ is derived that converges very fast to the required strain after one or two trials.

$$\overline{\varepsilon}_{cu} = \overline{\varepsilon}_{cc} \left[\frac{\dfrac{\overline{E_{sec}}}{\overline{E_{sec,u}}}\overline{r}}{\dfrac{\overline{c}}{\overline{\varepsilon}_{cu}} + 1} - \overline{r} + 1 \right]^{\frac{1}{\overline{r}}} \tag{4}$$

where $E_{sec,u} = \dfrac{f_{cu} - f_{cuo}}{\varepsilon_{cu} - 0.003}$, $c = \dfrac{f_{cuo} - E_{sec,u} \times 0.003}{E_{sec,u}}$.

2.2 Unconfined concrete analysis method

The analysis method of the unconfined concrete utilizes the finite layer procedure accounting for the concrete and steel using the concept of transformed section to determine the capacity under any ultimate strain profile.

The assumptions made in this analysis are:
(1) There is perfect bond between the longitudinal steel bars and the concrete.
(2) Strains along the depth of the column are assumed to be distributed linearly.
(3) Concrete stress in tension is neglected after cracking.
(4) The steel stress-strain relation is elastic-perfectly plastic.

The calculation of concrete force and moment can be summarized in the following steps:
(1) Dividing the section into a finite number of thin layers that have equal thickness.
(2) Determining the geometric properties of each layer (i.e., width (B_i), vertical distance to extreme compression fiber (Y_i) and to centerline of section ($Y_{\_i}$)).
(3) Using the pre assumed ultimate strain profile to determine the strain ε at layer mid-height (assuming that strain is constant through out the layer thickness).
(4) Calculating the compressive stress f_c from the strain using Hognestad's parabola.

$$f_c = f_c' \left(\frac{2\varepsilon_c}{\varepsilon_{co}} - \left(\frac{\varepsilon_c}{\varepsilon_{co}} \right)^2 \right) \tag{5}$$

(5) Finding the concrete layer force p_i, and moment m_i

$$p_i = f_{ci} \times B_i \times t \tag{6}$$

$$m_i = p_i \times Y_{\_i} \tag{7}$$

(6) Summing up the forces and moments to have the concrete force P_c and moment M_c.

$$P_c = \sum p_i \tag{8}$$

$$M_c = \sum m_i \tag{9}$$

The tensile stress is linear before cracking and is negligible beyond $7.5\sqrt{f_c'}$ in psi.

The calculation of reinforcing steel force and moment can be summarized in the following steps:

(1) Determining the geometric properties of each bar (i.e., the circumferencial angle of the bar location (θ_i) vertical distance to extreme compression fiber (Y_{si}) and to centerline of section (Y_{s_i})).

(2) Using the pre assumed ultimate strain profile and the bar location as found in the previous step, get the strain ε_{si}

(3) Calculating the stress f_{si}.

(4) Finding the force p_{si}, and moment m_{si}.

$$p_{si} = f_{si} \times A_{si} \tag{10}$$

$$m_{si} = P_{si} \times Y_{s\_i} \tag{11}$$

(5) Summing up the forces and moments to have the steel forces P_s and moment M_s

$$P_s = \sum p_{si} \tag{12}$$

$$M_s = \sum m_{si} \tag{13}$$

After getting the concrete and steel forces and moments, the section ultimate force and moment are found by simple addition. These two values represent a point coordinate on the interaction diagram (M, P). The full-unconfined concrete interaction diagram can be plotted by repeating this method for different strain profiles, Fig. 2. The smoothness of the interaction diagram can increase by running the analysis for more strain profiles imposing a number of intermediate points, Fig. 3. The inner curve represents the design limit after applying the resistance factors as per AASHTO-code provisions (AASHTO LRFD 2008).
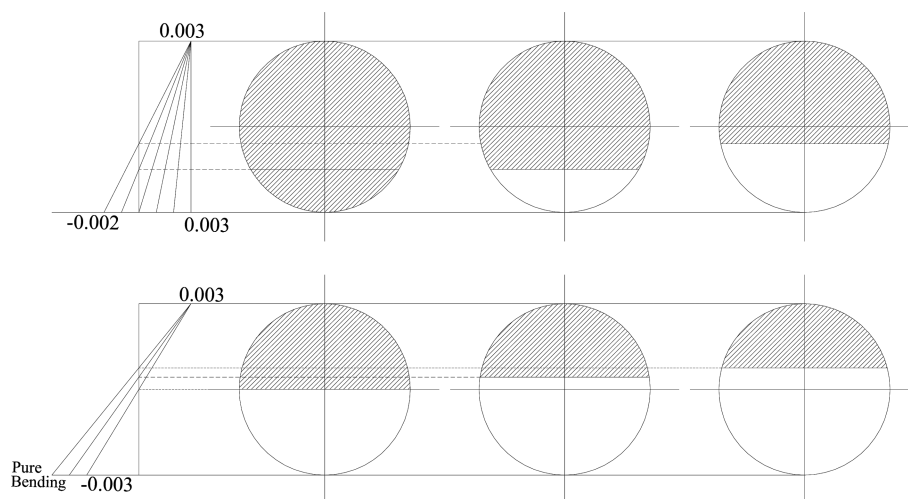

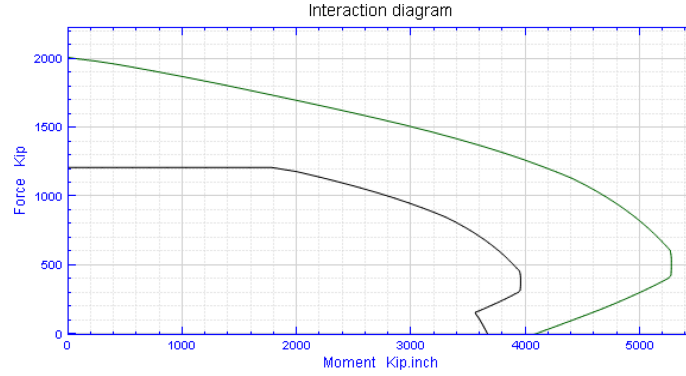Fig. 2 Different strain profiles for unconfined analysis

Fig. 3 Unconfined analysis and design interaction diagrams generated by the software

2.3 Confined concrete analysis method

Analysis of confined concrete is approached using incremental-iterative non-linear finite layer procedure. The material model necessitates considering constant eccentricity using the non-linear moment of area concept to achieve equilibrium points along the axial force-bending moment loading line up to failure. The assumptions of confined analysis are similar to those of unconfined analysis except for using Mander model adapted herein to the eccentricity equation for the concrete behavior in compression. The confined analysis procedure is described in the following steps, Figs. 4-5:

(1) Calculating the section initial properties:

Elastic axial rigidity EA

$$EA = \sum_i E_c B_i t + \sum_i (E_s - E_c) A_{si} \tag{14}$$

Elastic flexural rigidity about the elastic centroid EI

$$EI = \sum_i E_c B_i t (H - Y_i - Y_c)^2 + \sum_i (E_s - E_c) A_{si} (H - Y_{si} - Y_c)^2 \tag{15}$$
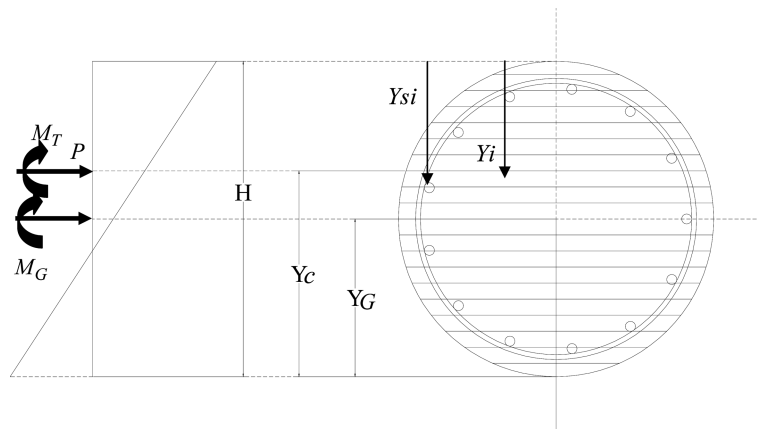

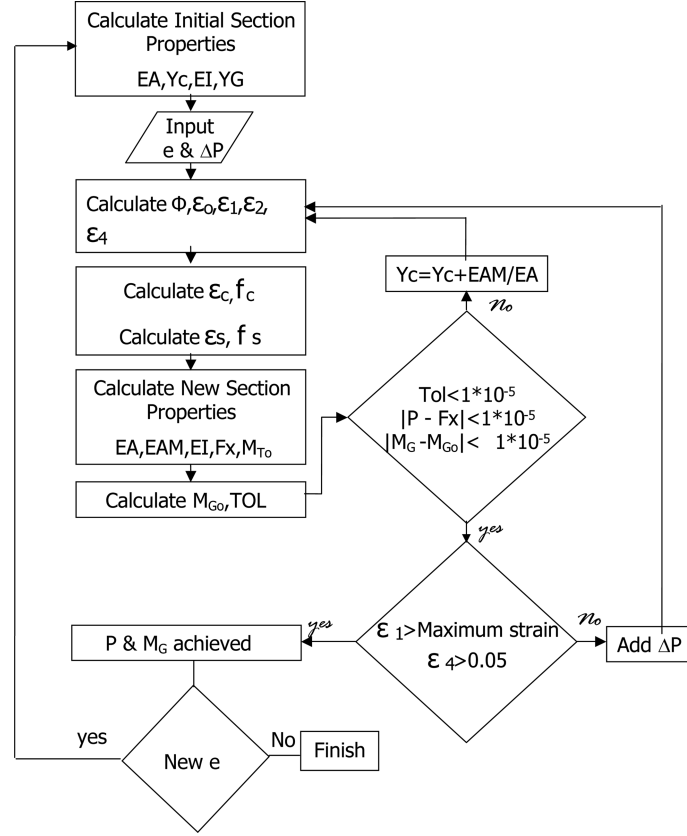Fig. 4 Idealized section, strain distribution and applied forces

Fig. 5 Flowchart for confined concrete nonlinear analysis

where the depth of the inelastic centroid position from the bottom fiber of the section (Y_c)

$$Y_c = \frac{\sum_i E_c B_i t(H-Y_i) + \sum_i (E_s - E_c)A_{si}(H-Y_{si})}{EA} \qquad (16)$$

The depth of the geometric section centroid position from the bottom fiber of the section (Y_G)

$$Y_G = \frac{H}{2} \qquad (17)$$

(2) Defining eccentricity e and axial load step ΔP.
(3) Computing the axial force and bending moment at the geometric centroid.

$$P = P + \Delta P, \ M_G = e \times P \qquad (18)$$

(4) Transferring moment to the current inelastic centroid

$$M_T = M_G + P \times (Y_G - Y_c) \qquad (19)$$

(5) Finding Curvature ϕ, strain at the inelastic centroid ε_o, the extreme compression fiber strain ε_1, the other extreme fiber strain ε_2 and at the extreme level of steel strain in tension ε_4

$$\phi = \frac{M_T}{EI}, \ \varepsilon_O = \frac{P}{EA} \tag{20}$$

$$\varepsilon_1 = \varepsilon_o + \phi(H - Y_c), \ \varepsilon_2 = \varepsilon_o - \phi Y_c \tag{21}$$

$$\varepsilon_4 = \varepsilon_o - \phi(Y_c - Cover) \tag{22}$$

(6) Calculating strain ε_c and corresponding stress f_c in each layer of concrete section by using the material model of Eq. (1)

$$\varepsilon_c = \varepsilon_1 - \phi Y_i$$

(7) Calculating strain ε_s and corresponding stress f_s in each bar.

(8) Calculating the new section properties *EA, EI, EAM* (moment of axial rigidity about inelastic centroid), F_x (internal axial force) and M_{To} (internal bending moment about the inelastic centroid)

$$EA = \sum_i E_{ci} B_i t + \sum_i (E_{si} - E_{ci}) A_{si} \tag{23}$$

$$EAM = \sum_i E_{ci} B_i t (H - Y_c - Y_i) + \sum_i (E_{si} - E_{ci}) A_{si} (H - Y_c - Y_{si}) \tag{24}$$

$$EI = \sum_i E_{ci} B_i t (H - Y_c - Y_i)^2 + \sum_i (E_{si} - E_{ci}) A_{si} (H - Y_c - Y_{si})^2 \tag{25}$$

$$F_x = \sum f_{ci} B_i t + \sum (f_{si} - f_{ci}) A_{si} \tag{26}$$

$$M_{To} = \sum f_{ci} B_i t (H - Y_c - Y_i) + \sum (f_{si} - f_{ci}) A_{si} (H - Y_c - Y_{si}) \tag{27}$$

(9) Transferring back the internal moment about the geometric centroid

$$M_{Go} = M_{To} - P(Y_G - Y_c) \tag{28}$$

(10) Checking the convergence of the inelastic centroid and equilibrium

$$TOL = EAM/(EA \times Y_c) \le 1 \times 10^{-5}$$

$$(P - F_x) \le 1 \times 10^{-5} \tag{29}$$

$$(M_G - M_{Go}) \le 1 \times 10^{-5}$$

(11) Updating the location of inelastic centroid, if necessary

$$Y_c = Y_c + \frac{EAM}{EA} \tag{30}$$

(12) Checking for the ultimate failure point

$$\varepsilon_1 = \overline{\varepsilon_{cu}} \ \text{ or } \ \varepsilon_4 = 0.05 \tag{31}$$

The framework of this procedure was originally developed by Rasheed and Dinno (1994) for rectangular reinforced concrete beam-columns.

3. Software development

The software is prepared using object oriented programming within the framework of the visual C-sharp language. This framework is adaptable to simulate a real process and it is flexible enough for efficient modifications and additions to the program.

As shown in Fig. 6, the main two classes are material, which has concrete and steel inherit from it, and shape that defines the cross section. The reinforced concrete circular cross section class is generated by combining the three classes; concrete, steel and circle. Numerical analyses are applied to this class by implementing any model (eccentricity model in this case). The software is called KDOT Column Expert.

3.1 Development of GUI

The Graphics User Interface is designed to offer visually compact style software integrating all input-output features of the program into a single-sheet format, Fig. 7. This is believed to be a
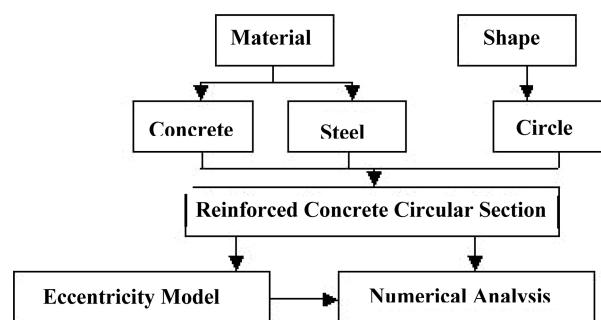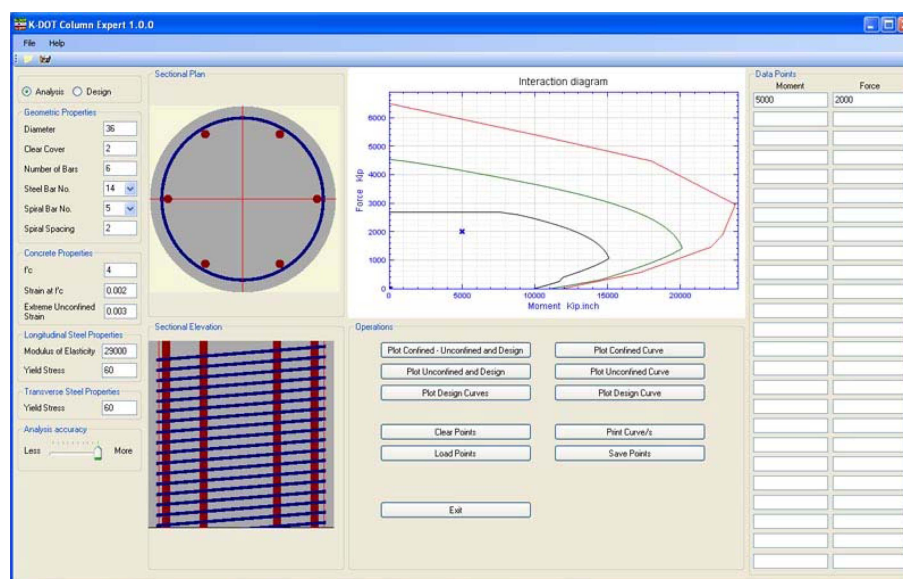

Fig. 6 Classes used to structure the program

Fig. 7 Interface layout of the software

powerful and unique feature of the software. The interface is outlined into five different sections as follows:

1. Data input: This section has a mode control that switches between Analysis input requirements and Design input requirements. The section is divided into four sub-sections:
   1.1. Geometric properties: These include the column diameter, clear cover, number of longitudinal bars, longitudinal bar size, spiral bar size and spiral spacing.
   1.2. Concrete properties: These include the concrete unconfined strength, strain corresponding to unconfined strength and ultimate unconfined strain.
   1.3. Longitudinal steel properties: These include modulus of elasticity and yield strength.
   1.4. Transverse steel properties: This sub-section is disabled for the design control. It includes the transverse steel modulus and yield strength in addition to the spiral or hoop control.
2. Detail drawing: This section automatically generates the sectional plan view and elevation view of the cross section as it is entered into the program. It gives the user a feel for the proportioning of the reinforcement sizes and spacing to avoid unrealistic input errors.
3. Capacity diagrams: This is the area where the resulting force-moment interaction diagrams are plotted.
4. Output Controls: This section has different buttons to control the capacity diagram results. One button has the option of plotting the design, unconfined ultimate and confined ultimate analysis diagrams together. Three more buttons plot those diagrams separately. Another button plots a series of design diagrams as explained in the following section. There are also buttons to save and load the example case as well as print the active diagram plot.
5. Demand Point Mapping: This section enables the user to input any number of demand force-moment points up to a maximum of 25. Once any point is input, it is immediately mapped on the diagram on display. This will facilitate the visual inspection of the design or analysis capacity satisfaction by the user.

3.2 Analysis and design features

The program is capable of analyzing the circular cross section in a variety of ways. First, the unconfined concrete interaction diagram is developed. Secondly, the resistance interaction diagram
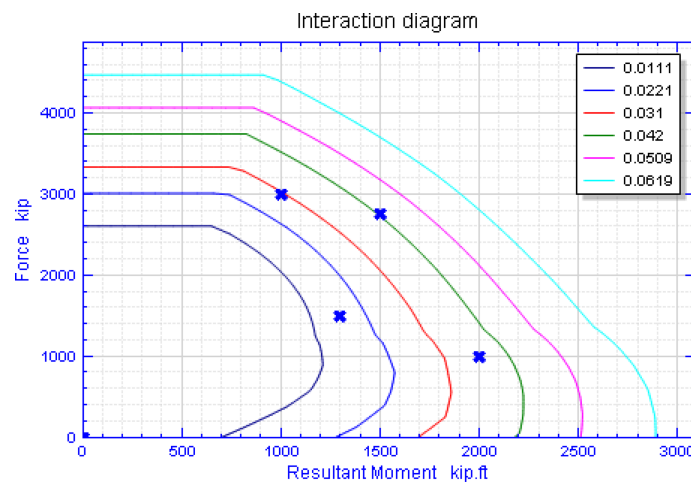

Fig. 8 Design option for AASHTO LRFD to quantify steel ratio

as per the AASHTO LRFD is generated. Finally, the actual capacity of the cross section is determined by taking into account the spiral or hoop confined effects and the concrete cover spalling beyond unconfined concrete crushing.

On the other hand, the software has the capability to plot several parallel design interaction diagrams according to AASHTO-LRFD, which disregard the confinement effect, for the same column size and different reinforcement ratios. This feature facilitates preliminary design by selecting the reinforcement ratio for which the curve is closest to the demand value, Fig. 8. The column size is changed and the process is repeated for the cases of extreme correspondence between the demand point and the generated curves. Fig. 8 presents the case of a 36 in. (914 mm) diameter column with a concrete cover of 2 in. (51 mm). The concrete strength selected is 4 ksi (27.6 MPa) and the steel yield strength is 60 ksi (414 MPa). It is evident from the demand values mapped on Fig. 8 that a steel ratio of 0.042 would satisfy the design resistance, which can be directly used to size the bars.

3.3 Software implementation

AASHTO LRFD (2008) does not give a lot of guidance to evaluate existing structures after a change of condition other than Article 3.6.5 titled vehicular collision force. KDOT has implemented the KSU Column Expert Program to evaluate the need for roadside barriers per ASSTHO LRFD Article 3.6.5. If the column has enough capacity then barrier is not required. KDOT bridge design manual section 3.5.1 describes this software and classifies the evaluation needed for redundant and non-redundant structures. For non-redundant structures, the capacity is limited to within the unconfined curve (*B*) region, Fig. 9. For redundant structures the capacity may be taken up to the fully confined curve (*C*) region, Fig. 9. For columns where the confined and unconfined capacities are similar in magnitude, the ductility of the column is reduced, limiting the reserve capacity. This reduction has lead to the development of the "75% rule", for non-redundant columns with little confinement reserve. For these columns, the capacity is limited to the minimum of the unconfined capacity or 75% of the distance between the design curve and the confined curve, Fig. 10. If the capacity, after the two above mentioned checks, is insufficient then barrier protection per *Article 3.6.5.1* or a crash wall or combination of the two will be required.
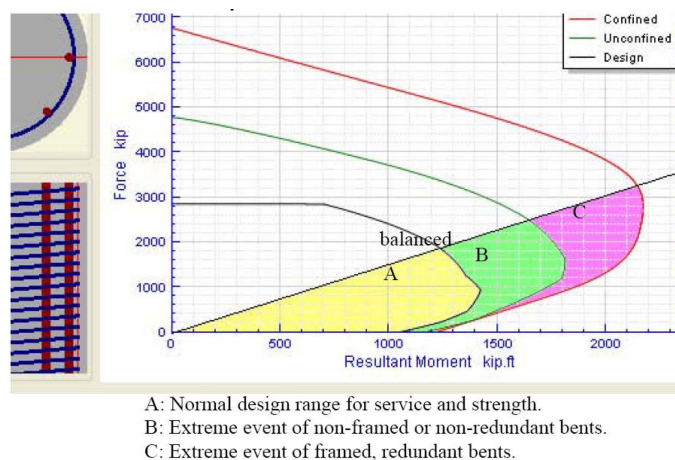

A: Normal design range for service and strength.
B: Extreme event of non-framed or non-redundant bents.
C: Extreme event of framed, redundant bents.

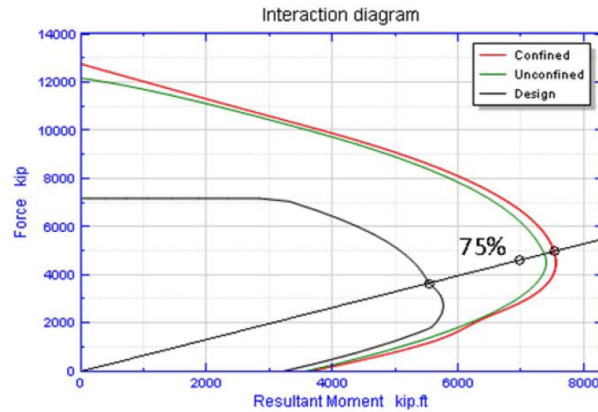Fig. 9 KDOT Bridge design manual's limits for redundancies

Fig. 10 KDOT column expert limits for 75% rule of non-redundant structure

4. Applications and results

The software is used to generate column interaction diagrams for AASHTO LRFD design requirements, unconfined compression analysis, confined compression analysis for eccentric loading with and without clear cover removal. To benchmark and evaluate the accuracy of the present software, the different analysis interaction diagrams are compared to (1) experimental data, (2) each other for an extreme case, (3) results from widely-used software for unconfined analysis and (4) results from using Mander model for the entire range of eccentricities, which are expected to be un-conservative. The following two cases of experimental data are compared first:

Case 1: Column tested by Mander *et al.* (1988b):

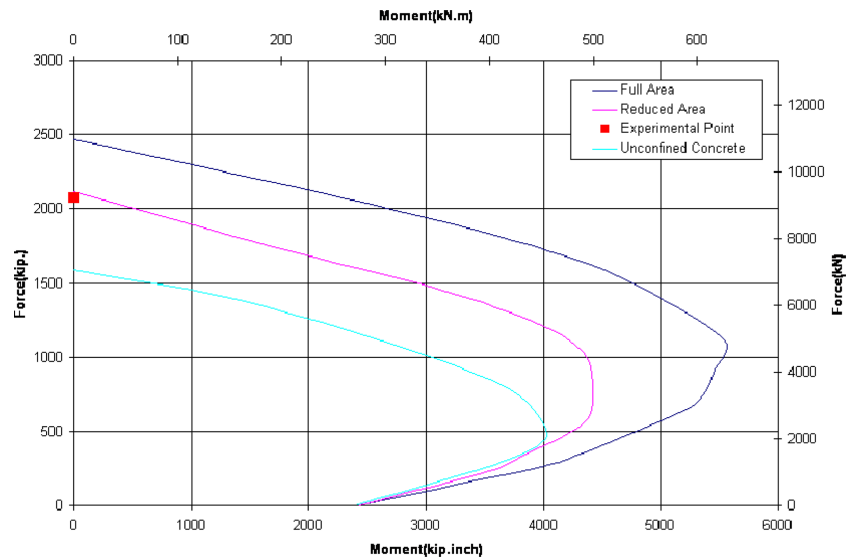Case 1 presents a circular column tested by Mander *et al.* (1988b) in pure axial compression. The

Fig. 11 Interaction diagrams of Case 1 by Mander *et al.* 1988

column has a diameter of 19.68 in (500 mm), a clear cover of 0.98 in (25 mm), and longitudinal reinforcement of 8 # 9 bars. The concrete strength is 4.49 ksi (31 MPa), and the steel yield strength is 42.9 ksi (296 MPa), for longitudinal reinforcement and 49.3 ksi (340 MPa), for spiral reinforcement. The spiral diameter is 0.472 in (12 mm), and the spiral spacing is 2.04 in (52 mm). The three interaction diagrams are shown in Fig. 11. The experimental data point matches very closely the middle curve that accounts for the cover spalling upon exceeding a compressive strain of 0.003. On the other hand, the full area curve accounts for the existence of the cover until the complete failure of the column, which is seen to be un-conservative. Accordingly, the confined analysis in the released software is based on the cover spalling whenever applicable.

Case 2: Columns tested by Esmaeily and Xiao (2004):

Case 2 illustrates circular columns investigated by Esmaeily and Xiao (2004), two in pure bending and one in combined bending and axial load. The column has a diameter of 16 in (406.4 mm), a clear cover of 0.512 in (13 mm), and longitudinal reinforcement of 12 # 4 bars. The concrete strength is 7.29 ksi (50.3 MPa), and the steel yield strength is 71 ksi (490 MPa), for longitudinal reinforcement and 68 ksi (469 MPa), for spiral reinforcement. The spiral diameter is 0.25 in (6.35 mm), and the spiral spacing is 1.26 in (32 mm). It is expected that the confinement effect is more pronounced than the previous case since the spiral spacing is significantly smaller. However, the diameter of the spiral reinforcement is noticeably smaller, which may balance the first effect.

The three interaction diagrams are seen, in Fig. 12, to be relatively close to each other near pure bending and the experimental data points matches very closely all curves at pure bending. The third experimental point, on the other hand, represents a case near the balanced point and yields all curves accurate and conservative enough.

Case 3: Benchmarking of confined analysis with zero f_{yh}:

This comparison was pursued to benchmark the results of two completely different algorithms when they should perform the same. The confinement analysis algorithm was used while assuming the yield strength in the transverse confining reinforcement to be equal to zero, which should yield an unconfined simulation. The unconfined computations are entirely independent, as presented
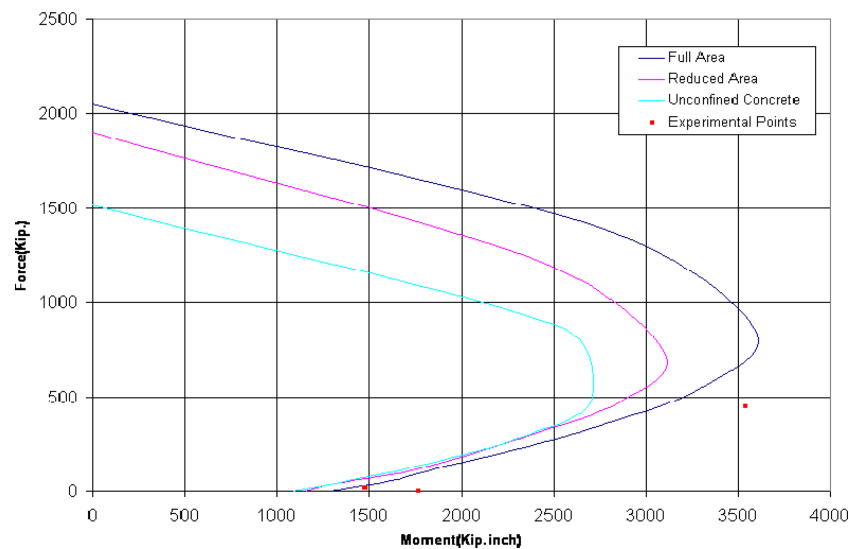

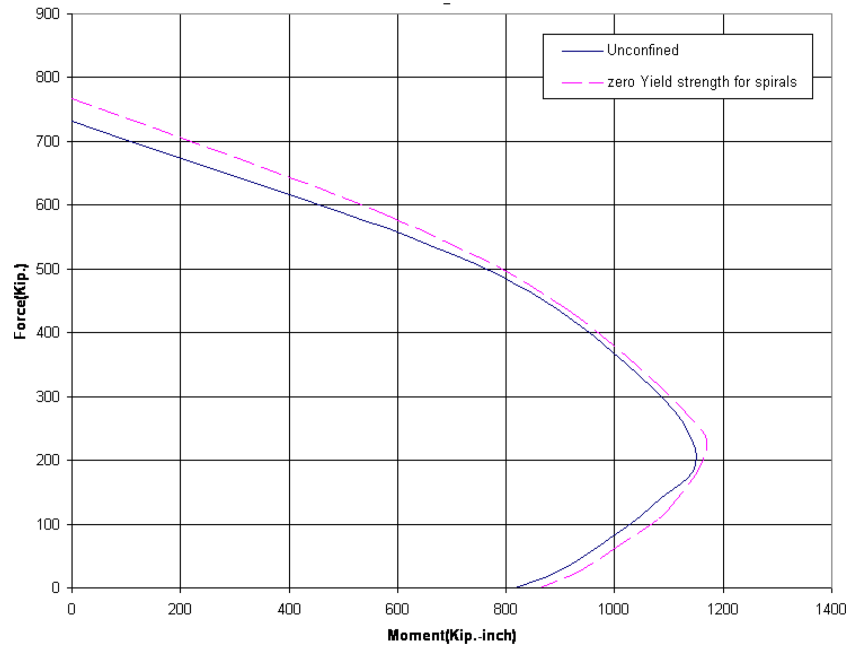Fig. 12 Interaction diagrams of Case 2 by Esmaeily and Xiao 2004

Fig. 13 Interaction diagrams for unconfined and confined analysis with $f_{yh}=0$

above. It is evident in Fig. 13 that the correlation between the two curves is excellent. This comparison obviously suggests the accuracy of the confined analysis algorithm.

Cases 4-6: Benchmarking of unconfined analysis with CSI-Section Builder Software:

To benchmark the unconfined compression analysis against widely-used software, three columns are compared against the corresponding results of CSI-Section Builder. The parameters of the first column are: A column diameter of 36 in (914.4 mm), a clear cover of 1.5 in (38.1 mm), and longitudinal reinforcement of 13 # 11 bars. The concrete strength is 4.0 ksi (27.6 MPa), and the steel yield strength is 60 ksi (413.7 MPa), for longitudinal and spiral reinforcement. The spiral reinforcement is #5 bars. The second case has a smaller column diameter with the following parameters: A column diameter of 25 in (635 mm), a clear cover of 1 in (25.4 mm), and longitudinal reinforcement of 12 # 10 bars. The concrete strength is 4.0 ksi (27.6 MPa), and the steel yield strength is 60 ksi (413.7 MPa), for longitudinal and spiral reinforcement. The spiral reinforcement is #4 bars. The third case has yet a smaller diameter of column with the following parameters: A column diameter of 20 in (508 mm), a clear cover of 1 in (25.4 mm), longitudinal reinforcement of 10 # 8 bars. The concrete strength is 4.0 ksi (27.6 MPa), and the steel yield strength is 60 ksi (413.7 MPa), for longitudinal and spiral reinforcement. The spiral reinforcement is #4 bars. The comparison for the three interaction diagrams of the three columns between the present program results and those of Section Builder is excellent, as shown in Fig. 14.

Case 7: Comparison with Mander concentric compression model:

To compare the predications of the present analysis against the well-known and widely used Mander model, the complete interaction diagram is generated using the Mander model, which is known to be valid for pure axial compression only, relative to the eccentricity model. The parameters of the column examined are a diameter of 23.65 in (600.71 mm), a clear cover of 0.8 in (20.3 mm), and longitudinal reinforcement of 16 # 8 bars. The concrete strength is 3.86 ksi (26.6
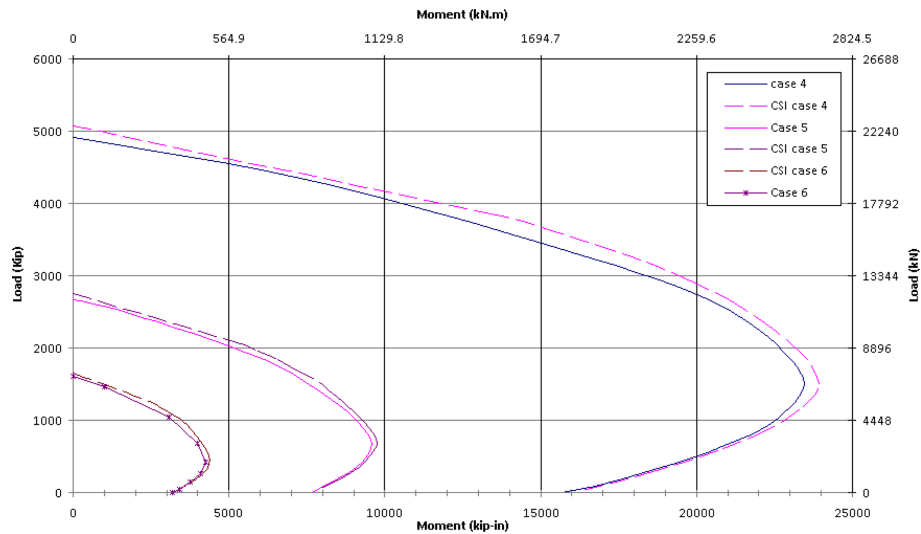
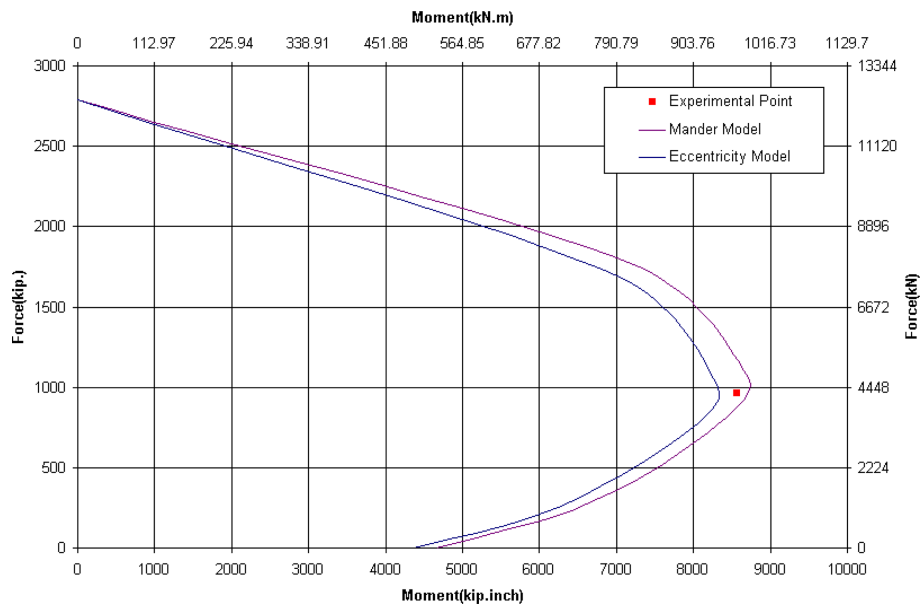Fig. 14 Comparison of unconfined analysis with CSI-Section Builder

Fig. 15 Interaction diagrams by the present model and Mander model

MPa) and the steel yield strength is 43.5 ksi (300 MPa) for the longitudinal and spiral reinforcement. The spiral diameter is 0.394 in (10 mm) and the spiral spacing is 1.97 in (50 mm). This column was tested by Fafitis and Shah (1985) and the experimental point is plotted against the two interaction diagrams in comparison. It is evident from the comparison, shown in Fig. 15, that the present model is very accurate and just conservative enough compared to the experimental point. On the other hand, the Mander model is shown to be accurate as well but not conservative enough relative to the experimental point.

5. Conclusions

In this work, a material model was developed for confined concrete circular columns subjected to eccentric loading. The model is directly extended from the widely known Mander model. Unconfined and confined analysis algorithms were written based on nonlinear behavior of circular reinforced concrete sections. These programs were integrated into interactive software to generate the complete series of design, unconfined and confined analysis interaction diagrams. The software is capable of mapping the demand values obtained from any structural analysis software onto the output diagrams to visually determine the adequacy of the analyzed, designed or evaluated columns. The software is benchmarked against experimental data, other software, itself and the Mander model to verify its reliability in providing accurate predictions. Improvements to KDOT Bridge Design Manual using this software with reference to AASHTO LRFD were made.

Acknowledgements

References

Aschheim, M., Gil-Martin, L.M. and Hernandes-Montes, E. (2011), "Proportioning of reinforced concrete column sections", *Eng. Struct.*, **33**(2), 685-688.

Anwar, N. and Qaasim, M. (2009), "Parametric study of reinforced concrete column cross-section for strength and ductility", *Key Eng. Mater.*, **400-402**, 269-274.

AASHTO (2008), "AASHTO LRFD bridge design specifications, interim", *American Association of State Highway and Transportation Officials.*

Balan, T.A., Spacone, E. and Kwon, M. (2001), "A 3D hypoplastic model for cyclic analysis of concrete structures", *Eng. Struct.*, **23**(4), 333-342.

Braga, F., Gigliotti, R. and Laterza, M. (2006), "Analytical stress–strain relationship for concrete confined by steel stirrups and/or FRP jackets", *J. Struct. Eng.-ASCE,* **132**(9), 1402-1416.

Carpinteri, A., Corrado, M., Goso, G. and Paggi, M. (2012), "Size-scale effects on interaction diagrams for reinforced concrete columns", *Constr. Build. Mater.,* **27**(1), 271-279.

Computers & Structures, Inc. (2006), "CSi Section Builder version 8.1.5", CSi, http://www.csiberkeley.com/products_SECTION.html.

Computers & Structures, Inc. (2011), "CSi COL version 8.3.2", CSi, http://www.csiberkeley.com/products_CSICOL.html.

Darwin, D. and Pecknold, D.A. (1977), "Nonlinear biaxial stress–strain law for concrete", *J. Eng. Mech.-ASCE,* **103**(2), 229-241.

Esmaeily, A. and Lucio, K. (2002), "Analytical performance of reinforced concrete columns using various analytical models: in international symposium of confined concrete, Xiao, Y., Kunnath, S. and Yi, W.", *Am. Concrete Inst.,* **238**, 95-110.

Esmaeily, A. and Xiao, Y. (2004), "Behavior of reinforced concrete columns under variable axial loads", *ACI Struct. J.,* **101**(1), 124-132.

Fafitis, A. and Shah, S.P. (1985), "Predictions of ultimate behavior of confined columns subjected to large deformations", *ACI J.,* **82**(4), 423-433.

Fam, A., Flisak, B. and Rizkalla, S. (2003), "Experimental and analytical modeling of concrete-filled fiber reinforced polymer tubes subjected to combined bending and axial loads", *ACI Struct. J.,* **100**(4), 529-539.

Kara, I.F. and Dundar, C. (2009a), "Prediction of deflection of reinforced concrete shear walls", *Adv. Eng. Softw.,* **40**(9), 777-785.

Kara, I.F. and Dundar, C. (2009b), "Effect of loading types and reinforcement ratio on an effective moment of inertia and deflection of a reinforced concrete beam", *Adv. Eng. Softw.,* **40**(9), 836-846.

Kim, Y.M., Kim, C.K. and Lee, J.C. (2009), "Rough set algorithm for crack category determination of reinforced concrete structures", *Adv. Eng. Softw.,* **40**(3), 202-211.

Kwon, M. and Spacone, E. (2002), "Three-dimensional finite element analyses of reinforced concrete columns", *Comput. Struct.,* **80**(2), 199-212.

Mander, J.B., Priestley, M.J.N. and Park, R. (1988a), "Theoretical stress-strain model for confined concrete", *J. Struct. Eng.-ASCE,* **114**(8), 1804-1826.

Mander, J.B., Priestley, M.J.N. and Park, R. (1988b), "Observed stress-strain behavior of confined concrete", *J. Struct. Eng.-ASCE,* **114**(8), 1827-1849.

Milton de Araújo, J. (2001), "Probabilistic analysis of reinforced concrete columns", *Adv. Eng. Softw.,* **32**(12), 871-879.

Oreta, A.W.C. and Ongpeng, J.M.C. (2011), "Modeling the confined compressive strength of hybrid circular concrete columns using neural networks", *Comput. Concrete,* **8**(5), 597-616.

Rasheed, H.A. and Dinno, K.S. (1994), "An efficient nonlinear analysis of R.C. sections", *Comput. Struct.,* **53**(3), 613-623.

Samra, R.M., Deeb, N.A. and Madi, U.R. (1996), "Transverse steel content in spiral concrete columns subject to eccentric loading", *ACI J.,* **93**(4), 412-419.

Song, Z. and Lu, Y. (2011), "Numerical simulation of concrete confined by transverse reinforcement", *Comput. Concrete,* **8**(1), 23-41.

Structure Point, LLC (2002-2011), "PCA Column version 4.10 or SP Column version 4.20", Structure Point: Concrete Software Solutions, http://www.structurepoint.org/soft/soft_profile.asp?l_family_id=30.

Tanyildizi, H. (2009), "Fuzzy logic model for the prediction of bond strength of high-strength lightweight concrete", *Adv. Eng. Softw.,* **40**(3), 161-169.

Tayem, A and Najmi, A. (1996), "Design of round reinforced concrete columns", *J. Struct. Eng.-ASCE,* **122**(9), 1062-1071.

Yeh, F.Y. and Chang, K.C. (2007), "Confinement efficiency and size effect of FRP confined circular concrete columns", *Struct. Eng. Mech.,* **26**(2), 127-150.

CC